Catalytic Evaluation of Hafnium Modified SiO_2 for the Dehydration of Alcohols

Heriberto Esteban Benito , Ricardo García Alamilla , Luz Arcelia García Serrano * , Francisco Paraguay Delgado , Juan Antonio Carmona García

Posted Date: 29 June 2023

doi: 10.20944/preprints202306.2024.v1

Keywords: Acidity; dehydration; ethylene; dimethyl ether

Article

Catalytic Evaluation of Hafnium Modified SiO_2 for the Dehydration of Alcohols

Heriberto Esteban Benito [1,7], Ricardo García Alamilla [2], Luz A. García Serrano [1,3,*], Francisco Paraguay Delgado [4] and Juan A. Carmona García [3,5,6]

[1] Centro Interdisciplinario de Investigaciones y Estudios sobre Medio Ambiente y Desarrollo-Instituto Politécnico Nacional, Ciudad de México, 07340, Estado de México, México ; h_esteban08@hotmail.com
[2] Tecnológico Nacional de México/Instituto Tecnológico de Ciudad Madero, Ciudad Madero, 89440, Tamaulipas, México; ricardo.ga@cdmadero.tecnm.mx
[3] Grupo de Investigación en Economía del Cuidado y Autonomía Económica, Ciudad de México, 11350, Estado de México, México; lugarcias@ipn.mx
[4] Centro de Investigación en Materiales Avanzados, Chihuahua, 31109, Chihuahua, México; francisco.paraguay@cimav.edu.mx
[5] Instituto Estatal de Relaciones Internacionales de Moscú MGIMO, Moscú, 119454, Rusia; futureteamexico@inbox.ru
[6] Escuela Superior de Comercio y Administración Unidad Santo Tomás-Instituto Politécnico Nacional, Ciudad de México, 11350, Estado de México, México
[7] Tecnológico Nacional de México/Instituto Tecnológico Superior de Naranjos, Naranjos, 92370, Veracruz, México; heriberto.esteban@itsna.edu.mx
* Correspondence: lugarcias@ipn.mx; Tel.: +52 55 3568 3894

Abstract: The influence of hafnium metal (Hf) and sulfate ions (SO_4^{-2}) on the acidic properties of SiO_2 mesopores synthesized by a non-hydrothermal method was studied using the following characterization techniques; TG-DTG, XRD, BET, SEM, TEM, EDS, FTIR, n-butylamine titration, FTIR-pyridine, and alcohol dehydration. The incorporation of 3.6% mol of Hf during the silicate synthesis step caused the characteristic structural arrangement of MCM-41 to collapse. However, an increase in the acid strength of the catalyst of up to 315 mV was observed, with Brönsted and Lewis-type acid sites being mostly present therein. Furthermore, the acidity of Hf- and (SO_4^{-2}) -modified SiO_2 in the dehydration of ethanol and methanol was evaluated, resulting in a selectivity towards ethylene and dimethyl ether, respectively. Acid solids have enormous potential to produce important compounds for the chemical industry using alternative routes other than petrochemical processes. They also represent a significant advance for biorefineries.

Keywords: acidity; dehydration; ethylene; dimethyl ether

1. Introduction

Since the discovery of mesoporous like MCM-41, MCM-48, HMS, and SBA-15, countless application possibilities have been opened for these materials in the field of heterogeneous catalysis, especially when metal atoms are introduced in the silicate structure, particularly organic and/or metallic species that promote interesting properties in silicates. In particular, textural properties are favored with increased specific area, uniform porosity, acidity, and thermal stability. These are some essential parameters that a solid material must meet for its application in catalytic reactions. The mesoporous silicate type MCM-41 meets these characteristics, with a hexagonal arrangement, surface area greater than 1000 m^2/g, and pore size of about 20 Å [1] facilitating the accessibility of bulky molecules to active sites and the rapid diffusion of reagents and products inside and outside the porous structure, leading to an increase in catalytic conversion which means a significant advantage over microporous materials, such as zeolites [2]. Nowadays, mesoporous silicates have been the subject of many studies to control their pore size, surface area, thermal stability, etc. However, their lack of acid sites limits their application as catalysts, but if a transition metal is introduced into the silicate structure, it generates a certain degree of acidity associated with the nature of the chemical

 doi:10.20944/preprints202306.2024.v1

bonds of the metal and silica [3]. Ti, Zr, Al, W, Mo, and Cr are among the most studied metal ions, which provide acidity to silicates of the M41S family [4–8]. A few numbers of studies have reported the influence of hafnium on the structural properties and catalytic behavior of MCM-41-type silicates. Generally, these studies focus on developing dielectric and micro electrical devices due to good thermal and mechanical stability and interfacial compatibility of hafnium with silicon [9–11]. On the other hand, hafnium oxide (HfO_2) shares physicochemical characteristics similar to those of zirconium oxide (ZrO_2) [12–14]. Ahmed et al. [15] reported that SO_4^{-2} ions promote stability of the tetragonal phase of ZrO_2, so it is expected that HfO2 will have the same behavior if SO_4^{-2} ions are introduced into the silicate structure. Bharali et al. [16] reported that doping SiO_2 with cerium and hafnium oxide increases thermal stability, acidity and/or basicity of the solid material. The acid-base nature of this material was evaluated in the decomposition of 4-methyl-2-pentanol into light olefins.

On the other hand, products from the dehydration of alcohols are a source of raw materials of high commercial value, such as light olefins and ethers that have been used as propellants, refrigerants, and fuels and could even be used as hydrogen sources for clean energy generation [17,18]. The present study reports the modification of an MCM-41 type silicate with Hf and SO_4^{-2} ions to promote acidity in the mesoporous silicate and its catalytic activity in the dehydration of alcohols.

2. Materials and Methods

2.1. Synthesis of Materials

Pure silicate was synthesized based on the methodology reported by Sepehrian et al. [19]. A known mass of cetyltrimethylammonium (CTABr, Aldrich, 99%), used as a structuring agent, and distilled water were mixed for 15 min under constant stirring. Subsequently, sodium silicate ($Na_2O_7Si_3$, Aldrich) was added and stirred for 30 min at room temperature. A 2M H_2SO_4 solution was added slowly dropwise to the resulting mixture until a pH of 9 was obtained and stirring continued for another 4 h under ambient conditions. The resulting precipitate was filtered, washed, and dried at 80 °C for 48 h, followed by a thermal process at 600 °C for 6 h under a flow of extra-dry air.

The introduction of hafnium atoms into the pure silicate was carried out during synthesis, at the stage after pH adjustment, at this stage a solution of hafnium tetrachloride ($HfCl_4$, Aldrich, 98%) was added slowly dropwise until 3.6 and 5.0% mol of metal on the silicate was obtained. The solution was stirred for a period of 4 h at room temperature. The filtering, drying, and calcination process of the Hf-modified SiO_2 was carried out under the same conditions used for the pure silicate. The resulting materials were labeled as; SiO_2, 3.6Hf/SiO_2, and 5.0Hf/SiO_2, respectively. A portion of the 3.6Hf/SiO_2 catalyst was sulfated with a theoretical content of 12 wt.% sulfate ions by the incipient moisture method and heat treated at 500 °C for 3 h in extra-dry air flow. This material was labeled as 12SHf/SiO_2.

The catalysts were characterized by thermal analysis using TA instruments STD 2690 Simultaneous DCS-TGA with a heating ramp of 5 °C min^{-1}, by X-ray diffraction at low angles on a SIEMENS D5000 diffractometer in the range of $1° < 2\theta < 10°$ with a scanning speed of 0.01° min^{-1} and diffraction patterns at $10° < 2\theta < 80°$ on a BRUKER AXS X diffractometer model D8 ADVANCE. Textural properties of the catalysts were determined by nitrogen physisorption in a Quantachrome model Autosorb-1 instrument. Fourier transform infrared spectroscopy was performed in the 400-4000 cm^{-1} range with 16 scans using an ATR cell in a Perkin Elmer Spectrum 100 spectrophotometer. Morphological characterization of the materials was carried out by scanning electron microscopy using a JEOL model 5800LV microscope and transmission electron microscopy using a Philips CM 200 microscope and a JEM-2200FS microscope with a spherical aberration corrector in STEM mode. The nature and acid strength of the solids were determined by pyridine adsorption using a Bruker Vector 22 FTIR spectrophotometer, and the acid strength of the sites was determined by potentiometric titration with n-butylamine. Finally, acidity of solids was evaluated through ethanol dehydration at 300, 325, and methanol dehydration at 350 °C. Catalytic activity tests were performed using a mass of 100 mg of catalyst in a microplant operating at atmospheric pressure and continuous

Preprints (www.preprints.org) | NOT PEER-REVIEWED | Posted: 29 June 2023 doi:10.20944/preprints202306.2024.v1

flow coupled to a Shimadzu-FID gas chromatograph equipped with a 30 m x 0.32 mm SPB-1 capillary column and 1 μm SUPELCO film.

3. Results and Discussion

3.1. Thermal Analysis

Thermogravimetric analysis (TG-DTG) results of the 3.6Hf/SiO_2 and 5.0Hf/SiO_2 precursors are shown in Figure 1. The total weight loss of the precursors occurred in three stages; in the first stage, weight loss occurred from room temperature to 150 °C due to removal of water physically adsorbed in the porous structure of the materials [20,21]. The second stage occurred between 150-400 °C, attributed to the decomposition of the structuring agent used in the synthesis [20–22]. At this temperature range, the weight loss of 3.6Hf/SiO_2 was 19.3% compared to that of 5.0Hf/SiO_2, which was 33.4% due to a higher loading of hafnium atoms, indicating that a large part of the structuring agent has been removed. De Souza et al. [20] reported that at this temperature range, oxidation of low molecular weight hydrocarbons occurs, generating CO_2, NO_2, and H_2O, as well as the elimination of surfactants. Finally, the last stage of weight loss was in the range of 400-600 °C, which corresponds to the evacuation of residues of organic compounds that strongly interact with inorganic species in the catalytic supports, as well as the condensation of silanol groups on the surface of the material [19,20]. On the other hand, the TG curve shows that the mesoporous silicate 5.0Hf/SiO_2 has a large amount of silanol groups coexisting at this temperature range, so a higher weight loss is attributed to dehydroxylation compared to the silicate 3.6Hf/SiO_2. The DTG curve shows signals attributed to the release of matter in the range of 50-600 °C related to the above-described stages associated with weight loss in the precursors.

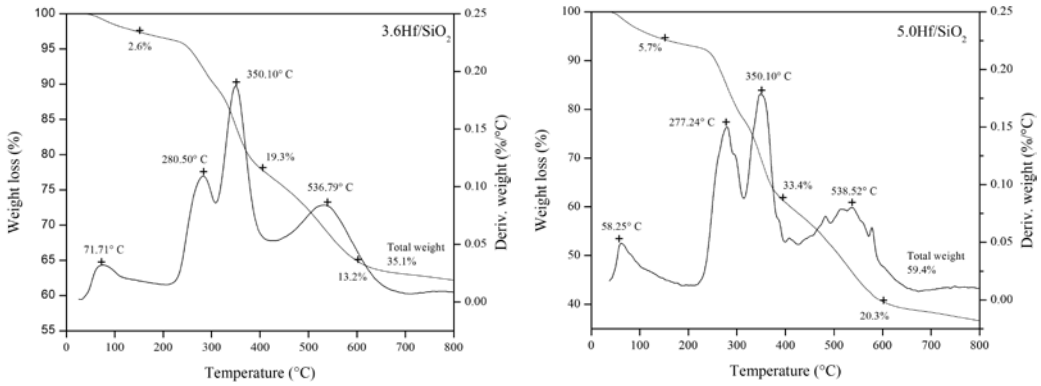

Figure 1. Thermal analysis of synthesized materials.

3.2. X-ray Diffraction

X-ray diffraction patterns at low angles are shown in Figure 2a. The pure material (SiO_2) shows a signal at 2.5° on the 2-theta scale (associated with the 100 plane) that characterizes a hexagonal arrangement similar to that reported for a mesoporous material of the M41S family [20], while for the 3.6Hf/SiO_2 material a broad peak is observed in the range of 1.5-3° on the 2 theta scale attributed to a poorly ordered structural arrangement. The structural arrangement observed in SiO_2 and 3.6Hf/SiO_2 collapses when these materials are impregnated with 12 wt.% sulfate ions and when a higher hafnium atom loading is added to SiO_2 in the synthesis step. On the other hand, Figure 2b, diffraction patterns between 20 and 80° on the 2-theta scale, shows hafnium-modified silicates with a broad peak at ~21° on the 2-theta scale, which characterizes an amorphous SiO2, additionally for pure silicate a peak at 31° on the 2-theta scale was observed, which corresponds to amorphous silica [23]. The Incorporation of Hf and SO_4^{-2} on pure SiO_2 promotes a decrease in peak intensity and broadening of said peak, attributed to the homogeneous incorporation of HfO_2 in the silicate structure since no signal of the metal oxide is identified. On the other hand, this behavior can also be attributed to the calcination temperature used, which prevented the formation of the crystalline phase of hafnium. Kim and Yong

Preprints (www.preprints.org) | NOT PEER-REVIEWED | Posted: 29 June 2023 doi:10.20944/preprints202306.2024.v1

[24] reported that the crystalline structure formation of HfO_2 requires calcination temperatures over 900 °C.

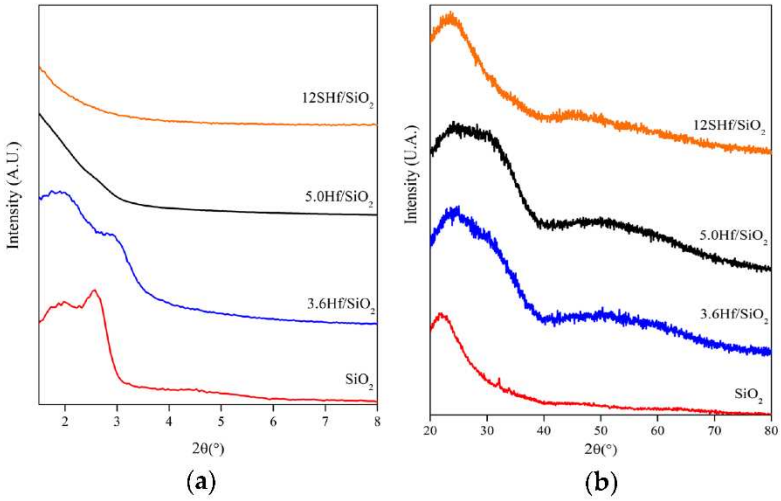

Figure 2. X-ray diffraction of catalysts: (**a**) low angles (1° ≤ 2θ ≤ 8°); (**b**) high angles (20° ≤ 2θ ≤ 80°).

3.3. Textural Properties

Figure 3a shows nitrogen adsorption-desorption isotherms of the Hafnium and sulfate ion-modified silicates. The $3.6Hf/SiO_2$ and $5.0Hf/SiO_2$ materials exhibit type-IV adsorption isotherms, confirming the mesoporosity of the solids [25], with pore sizes about 20-22 Å (Figure 3b). The presence of sulfate ions in the $12SHf/SiO_2$ material caused a change in the isotherm type to type III, which characterizes non-porous or macroporous solids with an average pore diameter around 64 Å. The increase in the average pore diameter is due to the destruction of the porous wall by the presence of sulfuric acid H_2SO_4, used as a source of SO_4^{-2} ions for the material. On the one hand, the acid strength of the catalyst increased, but as a result, the silicate structural arrangement collapsed, as observed in the X-ray diffractogram in Figure 2a.

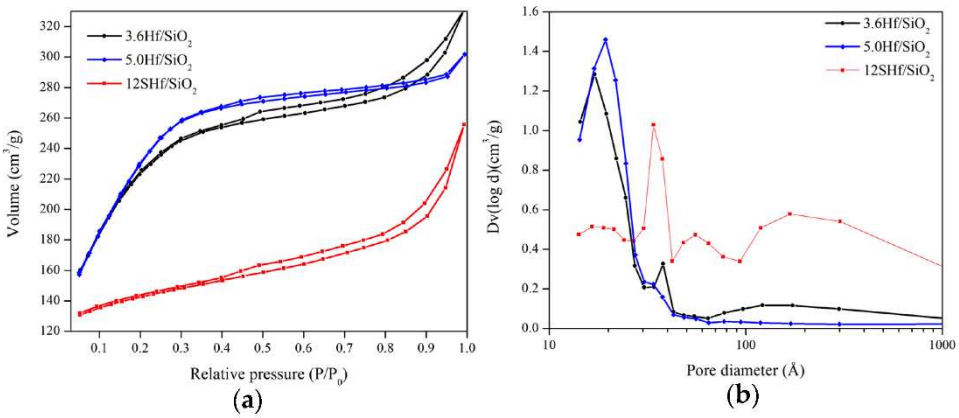

Figure 3. (**a**) Nitrogen adsorption isotherms; (**b**) pore size distribution.

Table 1 summarizes the textural parameters determined by the BET and BJH method. The specific area of $3.6Hf/SiO_2$ was 782 m^2g^{-1}, and the average pore diameter was 26 Å. By increasing the hafnium oxide content ($5.0Hf/SiO_2$), the specific area increases 50 m^2g^{-1}, which is attributed to the fact that the amorphous hafnium oxide has a certain degree of porosity contributing to the increase of the specific area of the composite. Also, a reduction in the average pore diameter and pore volume was observed, confirming a higher formation of amorphous crystals of HfO_2 on the external or internal surface of the silicate compared to $3.6Hf/SiO_2$. On the contrary, the specific area of $12SHf/SiO_2$ was

Preprints (www.preprints.org) | NOT PEER-REVIEWED | Posted: 29 June 2023 doi:10.20944/preprints202306.2024.v1

abruptly reduced to 152 m^2g^{-1} as well as the pore volume, however, the average pore diameter increased considerably compared to 3.6Hf/SiO_2 due to the presence of SO_4^{-2} ions on the walls of the hafnium silicate, which cause damage to the structural arrangement (Figure 3b).

Table 1. Textural properties of hafnium silicates.

Material	Area (m^2g^{-1})	Average Pore Diameter (Å)	Pore Volume (cm3/g)
3.6Hf/SiO_2	784	26	0.47
5.0Hf/SiO_2	831	22	0.45
12SHf/SiO_2	152	64	0.24

3.4. Scanning Electron Microscopy

Figure 4 shows the morphology of pure SiO_2, materials modified with 3.6 and 5% mol hafnium, and the material impregnated with 12 wt% sulfate ions. 5.0Hf/SiO2 and 12SHf/SiO_2 exhibit irregular morphologies with a tendency to agglomerate particles of variable size, forming large cavities between the agglomerates. Only 3.6Hf/SiO_2 shows a morphology of homogeneous particles similar to that observed in pure silicate. All the materials exhibited porosities classified as mesopores and macropores that correlate with the characterization results shown in Figure 3b.

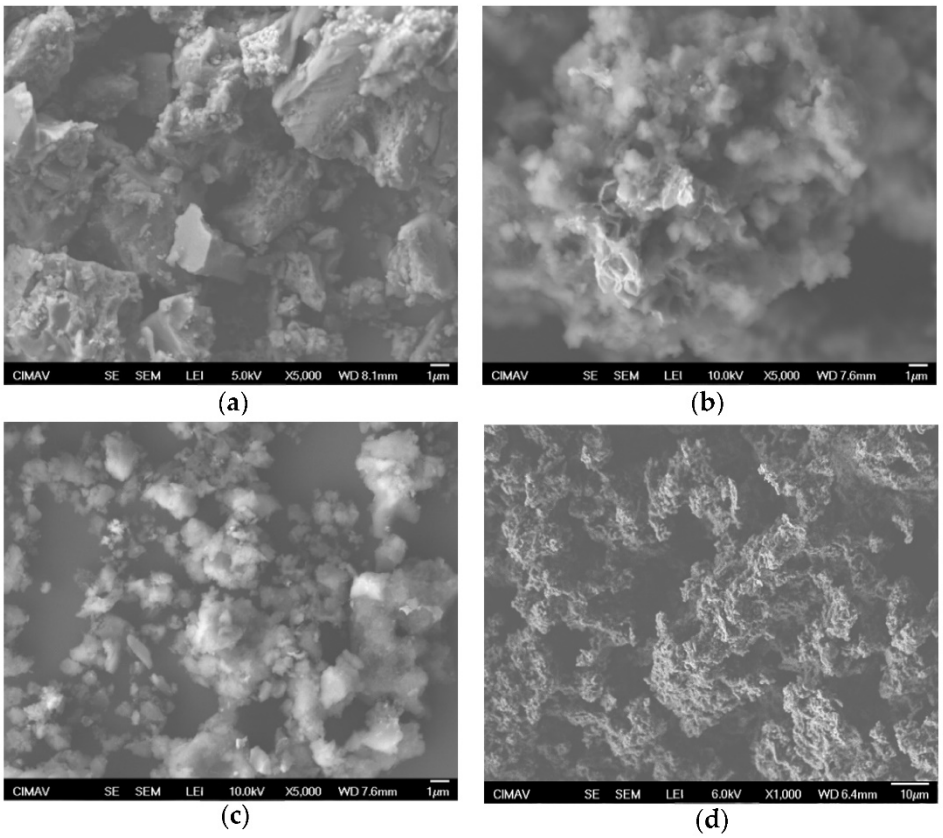

Figure 4. Scanning electron microscopy of hafnium silicates: (**a**) 5.0Hf/SiO_2; (**b**) 12SHf/SiO_2; (**c**) 3.6Hf/SiO_2; (**d**) SiO_2.

EDS analyses of 3.6Hf/SiO_2 and 12SHf/SiO_2 are shown in Figure 5, both samples comprising Si, O, and Hf. Additionally, sulfur (S) was identified in the spectrum of the 12SHf/SiO_2 material, corresponding to the presence of SO_4^{-2} ions used to increase the acid strength of 3.6Hf/SiO_2. Hong et al. [26] carried out an EDS analysis on MCM-41 showing elemental compositions of silicon (Si) and oxygen (O) similar to those observed in these spectra. Table 2 shows the atomic percentage of the elements constituting the catalysts. This quantification of elements was carried out in different

Preprints (www.preprints.org) | NOT PEER-REVIEWED | Posted: 29 June 2023 doi:10.20944/preprints202306.2024.v1

sections of the samples, showing that Hf and S are not homogeneously distributed. However, as the analysis confirmed the presence of Hf (3.42%), the amorphous structural form of HfO_2 is verified.

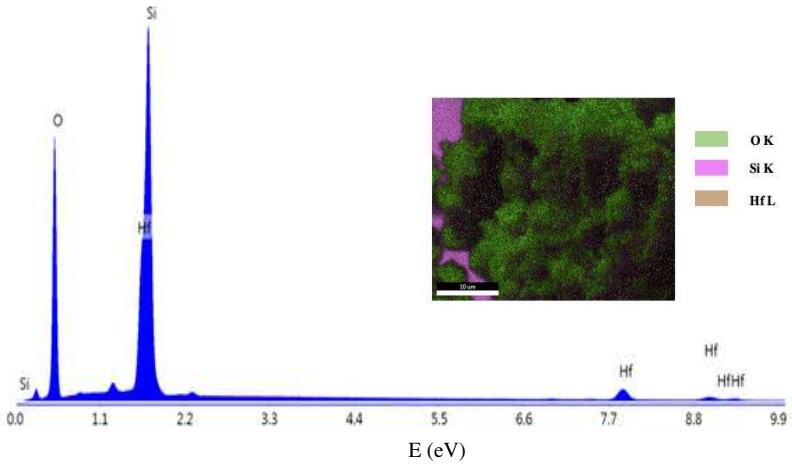

(**a**)

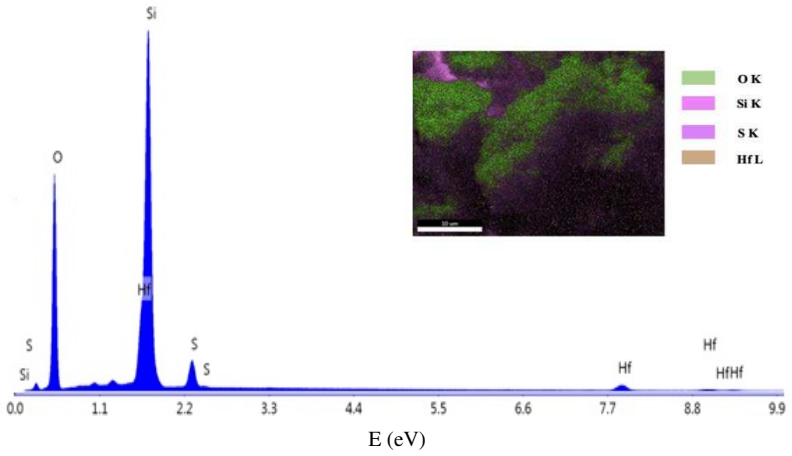

(**b**)

Figure 5. EDS analysis of hafnium silicate and sulfated hafnium silicate: (**a**) 3.6Hf/SiO_2; (**b**) 12SHf/SiO_2.

Table 1. Elemental composition of the catalysts.

3.6Hf/SiO_2		**12Hf/SiO_2**	
Element	**Atomic (%)**	**Element**	**Atomic (%)**
O K	65.44	O K	61.90
Si K	30.58	Si K	31.31
Hf L	3.98	Hf L	3.42
		S K	3.37

3.5. Transmission Electron Microscopy

Figure 6 shows the micrograph of the synthesized catalysts. SiO_2 shows a structural arrangement consisting of uniform channels similar to that reported by for a mesoporous MCM-41 type silicate. However, the signals of the (110) and (200) planes obtained by XRD of the pure mesoporous silicate are not well defined, thus confirming that the material has an incipient structural arrangement similar to MCM-41 but poorly ordered. On the other hand, the presence of 3.6% mol of Hf in the silicate caused the loss of the structural ordering observed in the SiO_2 micrograph due to the formation of

Preprints (www.preprints.org) | NOT PEER-REVIEWED | Posted: 29 June 2023 doi:10.20944/preprints202306.2024.v1

amorphous HfO_2. Higher metal loadings lead to amorphous structured materials. This same behavior was also observed with the 3.6Hf/SiO_2-sulfate material directly impregnated with 12 wt% SO_4^{-2} ions.

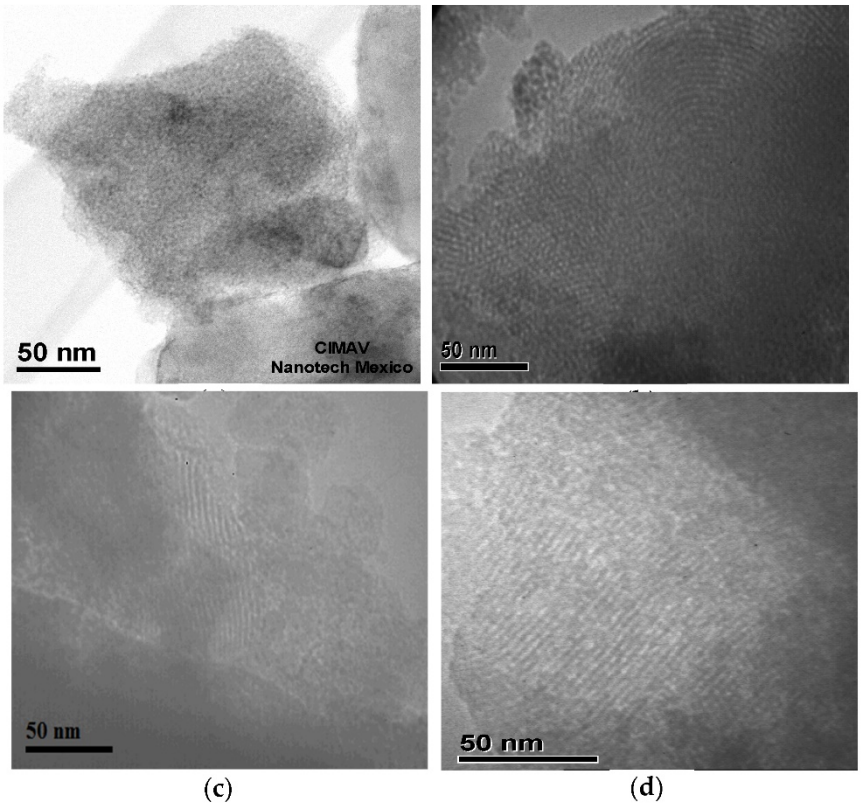

Figure 6. Transmission electron micrograph of the catalysts: (**a**) 5.0Hf/SiO_2; (**b**) 12SHf/SiO_2; **(c)** 3.6Hf/SiO_2; (**d**) SiO_2.

3.6. FTIR Spectroscopy

Infrared spectra of the synthesized materials are shown in Figure 7. All three materials have signals at 460 cm^{-1}, corresponding to metal-oxygen bonds, specifically Si-O and Hf-O bonds [13,23,27]. Inverted peaks at 810 and 1080 cm^{-1} correspond to symmetrical and asymmetrical molecular vibrations of Si-O-Si bonds [1]. O'Dell et al. [11] reported that the Si-O-Hf bond is located at 960 cm^{-1}. However, there is an overlap with a broad band at 1080 cm^{-1}, which corresponds to Si-O-Si bond vibrations, not allowing for a clear Si-O-Hf bond identification. However, the IR spectrum of the 5Hf/SiO_2 material showed a band of higher intensity in this region that confirmed the presence of Hf bonded to oxygen and silicon, which is supported by the EDS analysis results (Figure 5). On the other hand, the IR spectrum of the 12SHf/SiO_2 material shows two bands: a first band overlapped in the region of 1000-1200 cm^{-1}, and a second band, although of very low intensity, observed in the region of 600-620 cm^{-1}. Guo and Wang [28] reported comparable results for Na_2SO_4/SiO_2 with a spectrum showing symmetric tension vibrations at 617 y 1126 cm^{-1} corresponding to S-O bonds. In addition to the FT-IR analysis, an IR spectrum of sodium sulfate (Na_2SO_4) was added as reference to support the presence of sulfate ions in the 12SHf/SiO_2 material as observed in the EDS analysis (Figure 5).

Preprints (www.preprints.org) | NOT PEER-REVIEWED | Posted: 29 June 2023 doi:10.20944/preprints202306.2024.v1

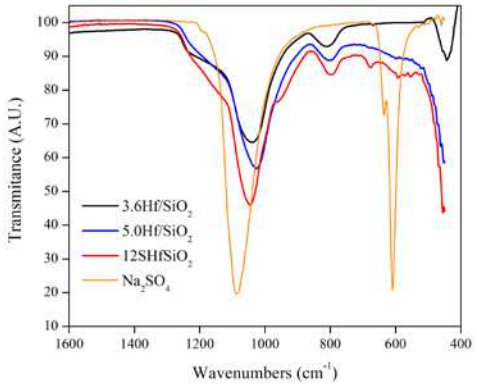

Figure 7. FTIR spectroscopy of the catalysts.

3.7. Potentiometric Titration with n-Butylamine

Maximum Acid Strength (M.A.S.) of catalysts was determined by potentiometric titration with n-butylamine. The first reading recorded, in mV, indicates the acidic character of the materials. Pizzio et al. [29] lassified surface acidity of solid catalysts into very strong acid sites (E > 100 mV), strong acid sites (0 < E < 100 mV), weak acid sites (-100 < E < 0 mV), and very weak acid sites (E < -100 mV). Figure 8 shows the M.A.S. developed by SiO_2, 3.6Hf/SiO_2 and 12SHf/SiO_2. SiO_2 lacks acid sites, which is confirmed by the -42-mV reading, but when hafnium was introduced into the silicate the surface acid strength of the material increased to 321 mV. The higher the hafnium oxide content, the higher the M.A.S. On the other hand, sulfate ions impregnated in the 3.6Hf/SiO_2 material cause a significant increase in the acidity of the catalyst. From these results it is inferred that catalysts 3.6Hf/SiO_2 and 12SHf/SiO_2 will be promising for carrying out acidity-demanding reactions, such as alcohol dehydration and other reactions like those typically found in petroleum refineries.

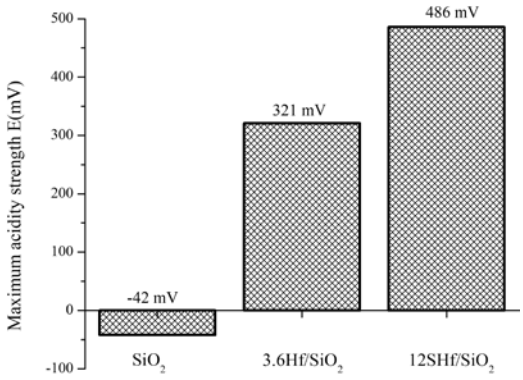

Figure 8. Maximum acid strength of catalysts determined by potentiometric titration with n-butyl amine.

3.8. FTIR-Pyridine Spectroscopy

The nature of acid sites of the catalysts was determined by IR spectroscopy with adsorption-desorption of pyridine (Figure 9). IR-pyridine spectra of 3.6Hf/SiO_2 show Lewis-type signals at 1445 and 1609 cm^{-1}, while 12SHf/SiO_2 exhibited signals at 1580 and 1595 cm^{-1}, which are associated with a solid with Lewis's acid sites. Said acidity is attributed to the presence of hafnium atoms within the pores of the SiO_2 [15,30]. Both materials exhibited peaks at 1544, 1637, and 1490 cm^{-1} corresponding to Brönsted-type acid sites and Lewis-Brönsted-type acid sites [30]. Catalyst 12SHf/SiO_2 exhibited very strong acid sites compared to catalyst 3.6Hf/SiO_2, as the amount of pyridine retained could still be observed at temperatures above 400 °C.

Preprints (www.preprints.org) | NOT PEER-REVIEWED | Posted: 29 June 2023 doi:10.20944/preprints202306.2024.v1

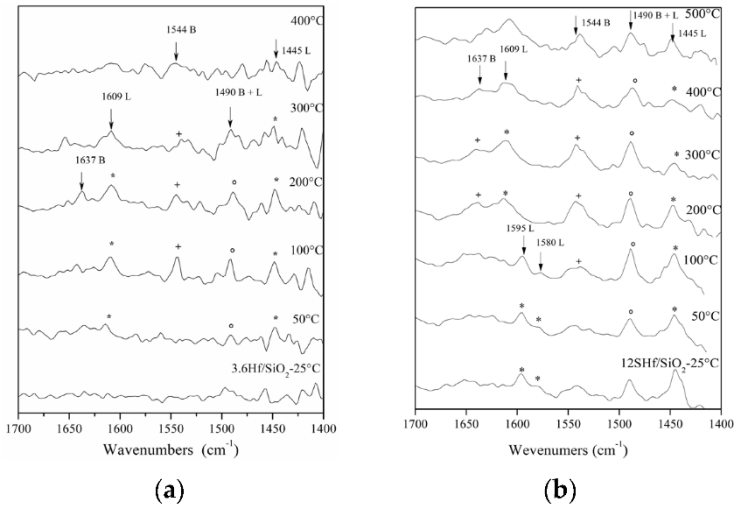

Figure 9. FT-IR spectroscopy with adsorption-desorption of pyridine **(a)** Hf/SiO_2; **(b)** 12SHf/SiO_2.

3.9. Catalytic Activity

3.9.1. Ethanol Dehydration

Ethanol was used as a model molecule to determine the acid-base nature of SiO_2, 3.6Hf/SiO_2, and 12SHf/SiO_2. The dehydration reaction of ethanol was carried out in an inert atmosphere. Dehydration can be performed through three possible pathways: 1) intra-molecular dehydration to produce ethylene, 2) intermolecular dehydration to generate diethyl ether, and 3) dehydrogenation of the alcohol to produce acetaldehyde [31,32], and as a result, a reaction selectivity parameter depending on the relative number of active site types in the catalyst is obtained. Table 3 summarizes the results of the ethanol dehydration reaction with selectivity to ethylene and diethyl ether at different temperatures. SiO_2 did not show catalytic activity as it lacks acid sites, as demonstrated in the potentiometric titration test with n-butylamine (Figure 8). When Hafnium is present in the silicate alcohol decomposition is favored, however, at low temperatures ethanol conversion is lower than 50% with a tendency to form diethyl ether, conversely, when the reaction temperature is increased, selectivity of alcohol conversion to ethylene is increased as reported in literature [31,33]. According to the results obtained by titration with n-bta and pyridine adsorption, 12SHf/SiO2 contains very strong acid sites. Therefore, they are responsible for ethanol dehydration at low temperatures. At 300 °C ethanol conversion was 100% with selectivity to ethylene. It should be noted that, in alcohol dehydration processes, the reaction temperature is a key factor to consider since a slight change in this operating variable can significantly affect the selectivity of the alcohol dehydration reaction. In the present study, no products generated by ethanol dehydrogenation were identified, confirming that hafnium-modified silicates either lack basic sites or are too weak to carry out a dehydrogenation reaction. On the other hand, the ethanol dehydrogenation reactions were carried out for 3 h, the catalysts showed good thermal stability in the course of the reaction, and no deactivation by organic carbon deposition was observed.

Table 3. Catalytic activity of the materials.

Catalyst	T = 300 °C			T = 325 °C			T = 350 °C		
	X_A* (%)	$S_{C_2^=}$** (%)	S_E*** (%)	X_A (%)	$S_{C_2^=}$ (%)	S_E (%)	X_A (%)	$S_{C_2^=}$ (%)	S_E (%)
SiO_2	0	0	0	0	0	0	0	0	0
3.6Hf/SiO_2	50	86	14	80	96	4	94	99	1
12SHf/SiO_2	100	100	0	-	-	-	-	-	-

* Conversion. ** Selectivity to ethylene. *** Selectivity to diethyl ether.

Preprints (www.preprints.org) | NOT PEER-REVIEWED | Posted: 29 June 2023 doi:10.20944/preprints202306.2024.v1

Additionally, the catalytic behavior of methanol dehydration was studied, which can decompose intramolecularly or intermolecularly depending on the reaction conditions and the type of catalyst [34]. Methanol dehydration reaction requires catalysts with strong acid sites, and as observed in the pyridine adsorption-desorption tests (Figure 9) and ethanol dehydration tests (Table 3), 3.6Hf/SiO_2 and 12SHf/SiO_2 have very strong acid sites suitable for catalyzing decomposition reactions of said molecule. Figure 10a shows ethanol conversion over catalyst 3.6Hf/SiO_2 at 340 °C, with 30% ethanol conversion and dimethyl ether as the main product. The reaction was carried out for 240 min without deactivation of the material. Catalyst 12SHf/SiO_2 exhibited higher methanol conversion, up to 70%, but selectivity to dimethyl ether was lower compared to 3.6Hf/SiO_2. This is attributed to a decrease in the number of very strong acid sites in 12SHf/SiO_2 over the course of the reaction, resulting in lower selectivity to the formation of hydrocarbon compounds (Figure 10b) [35]. This reduction in acid sites is attributed to coke deposition on the catalyst surface, however conversion reaction and selectivity to dimethyl ether remained stable for 200 min.

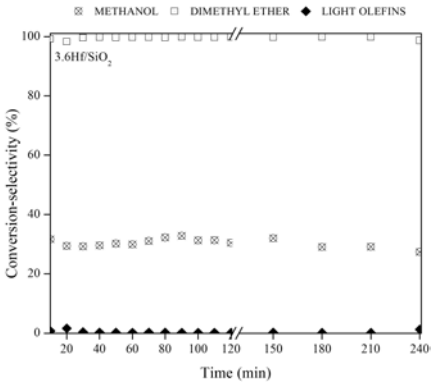

Figure 10. Methanol dehydration: (**a**) 3.6Hf/SiO_2 and (**b**) 12SHf/SiO_2 at 340 °C.

4. Conclusions

Mesoporous silicon oxide with a structure similar to MCM41 was prepared from sodium silicate, and its surface acidity was modified by adding 3.6 wt.% hafnium as well as sulfate ions. However, the introduction of sulfate ions from sulfuric acid caused the hexagonal structure, which is characteristic of MCM-41 materials, to collapse as evidenced by X-ray analysis at low angles. However, synergy between sulfate ions and hafnium was evidenced by the high catalytic activity obtained in the decomposition of ethanol and methanol. These materials showed resistance to deactivation during the reaction, making them a good option for the decomposition of bio-alcohols into high-value-added products.

Supplementary Materials: Not applicable.

Author Contributions: Conceptualization, H.E.B and R.G.A.; formal analysis, H.E.B and R.G.A.; investigation, H.E.B.; methodology, H.E.B., and R.G.A.; software, F.P.D. and L.A.G.S.; supervision, R.G.A; validation, R.G.A. and L.A.G.S.; writing—original draft, H.E.B.; writ- ing—review and editing, R.G.A., L.A.G.S., J.A.C.G and F.P.D. All authors have read and agreed to the pub- lished version of the manuscript.

Funding: Not applicable.

Institutional Review Board Statement: Not applicable.

Informed Consent Statement: Not applicable.

Acknowledgments: To the Consejo Nacional de Humanidades, Ciencias y Tecnologías (CONAHCYT) and Instituto Tecnológico Superior de Naranjos. We want to express our gratitude to Luis de la Torre, Ernesto Guerrero, and Wilber Antúnez from the Advanced Materials Research Center for their support in the characterization of the materials, as well as to Cinthya Cristal Casanova Juárez.

Conflicts of Interest: The authors declare no conflict of interest.

References

1. Dhengale, S.D.; Bhosale, T.R.; Shinde, S.B.; Rode, C.V.; Kolekar, G.B.; Anbhule, P.V. An Efficient and Convenient Heterogeneous Cu/MCM-41 Catalyst for the Synthesis of 7,10,11,12-Tetrahydrobenzo[c]Acridin-8(9H)-One Derivatives. *Res. Chem. Intermed.* **2023**, *49*, 1581–1600, doi:10.1007/s11164-023-04962-3.
2. Afanasiev, P.; Thiollier, A.; Breysse, M.; Dubois, J.L. Control of the Textural Properties of Zirconium Oxide. *Top. Catal.* **1999**, *8*, 147–160, doi:10.1023/A:1019109127118.
3. Du, Y.; Sun, Y.; Di, Y.; Zhao, L.; Liu, S.; Xiao, F.-S. Ordered Mesoporous Sulfated Silica-Zirconia Materials with High Zirconium Contents in the Structure. *J. Porous Mater.* **2006**, *13*, 163–171, doi:10.1007/s10934-006-7026-5.
4. Claure Zeballos, M.; Pardo Tarifa, F.L.; Lopez N., L.G.; Cabrera M., S. Mesoporous Silicoaluminate Materials (MCM-41, SBA-15 And MCF) By Atrane Route For Cobalt Catalyst. *Rev. Boliv. Quím.* **2022**, *39*, doi:10.34098/2078-3949.39.4.2.
5. Jiménez-Morales, I.; Santamaría-González, J.; Maireles-Torres, P.; Jiménez-López, A. Zirconium Doped MCM-41 Supported WO_3 Solid Acid Catalysts for the Esterification of Oleic Acid with Methanol. *Appl. Catal. Gen.* **2010**, *379*, 61–68, doi:10.1016/j.apcata.2010.03.001.
6. Naik, S.P.; Bui, V.; Ryu, T.; Miller, J.D.; Zmierczak, W. Al-MCM-41 as Methanol Dehydration Catalyst. *Appl. Catal. Gen.* **2010**, *381*, 183–190, doi:10.1016/j.apcata.2010.04.007.
7. Wang, Y.; Guo, Y.; Wang, G.; Liu, Y.; Wang, F. Synthesis, Characterization and Catalytic Activities of Bimetallic Modified MCM-41 for Epoxidation of Styrene. *J. Sol-Gel Sci. Technol.* **2011**, *57*, 185–192, doi:10.1007/s10971-010-2340-4.
8. Xie, C.; Liu, F.; Yu, S.; Xie, F.; Li, L.; Zhang, S.; Yang, J. Catalytic Cracking of Polypropylene into Liquid Hydrocarbons over Zr and Mo Modified MCM-41 Mesoporous Molecular Sieve. *Catal. Commun.* **2008**, *10*, 79–82, doi:10.1016/j.catcom.2008.08.001.
9. Broqvist, P.; Pasquarello, A. Amorphous Hafnium Silicates: Structural, Electronic and Dielectric Properties. *Microelectron. Eng.* **2007**, *84*, 2416–2419, doi:10.1016/j.mee.2007.04.013.
10. Kopani, M.; Mikula, M.; Pinčík, E.; Kobayashi, H.; Takahashi, M. FT IR Spectroscopy of Nitric Acid Oxidation of Silicon with Hafnium Oxide Very Thin Layer. *Appl. Surf. Sci.* **2014**, *301*, 24–27, doi:10.1016/j.apsusc.2014.01.124.
11. O'Dell, L.A.; Gunawidjaja, P.N.; Holland, M.A.; Mountjoy, G.; Pickup, D.M.; Newport, R.J.; Smith, M.E. Characterisation of Sol–Gel Prepared $(HfO_2)x(SiO_2)1-x$ (X=0.1, 0.2 and 0.4) by ^{1}H, ^{13}C, ^{17}O and ^{29}Si MAS NMR, FTIR and TGA. *Solid State Nucl. Magn. Reson.* **2008**, *33*, 16–24, doi:10.1016/j.ssnmr.2007.11.001.
12. Ahmed, M.A. Surface Characterization and Catalytic Activity of Sulfated-Hafnia Promoted Zirconia Catalysts for n-Butane Isomerization. *Fuel Process. Technol.* **2011**, *92*, 1121–1128, doi:10.1016/j.fuproc.2011.01.008.
13. Khatri, C.; Mishra, M.K.; Rani, A. Synthesis and Characterization of Fly Ash Supported Sulfated Zirconia Catalyst for Benzylation Reactions. *Fuel Process. Technol.* **2010**, *91*, 1288–1295, doi:10.1016/j.fuproc.2010.04.011.
14. Jakóbik-Kolon, A.; Bok-Badura, J. Stripping of Hafnium and Zirconium from Chelating Ion-Exchange Resin. *Polyhedron* **2022**, *224*, 116023, doi:10.1016/j.poly.2022.116023.
15. Ahmed, A.I.; El-Hakam, S.A.; Samra, S.E.; EL-Khouly, A.A.; Khder, A.S. Structural Characterization of Sulfated Zirconia and Their Catalytic Activity in Dehydration of Ethanol. *Colloids Surf. Physicochem. Eng. Asp.* **2008**, *317*, 62–70, doi:10.1016/j.colsurfa.2007.09.043.
16. Bharali, P.; Thrimurthulu, G.; Katta, L.; Reddy, B.M. Preparation of Highly Dispersed and Thermally Stable Nanosized Cerium–Hafnium Solid Solutions over Silica Surface: Structural and Catalytic Evaluation. *J. Ind. Eng. Chem.* **2012**, *18*, 1128–1135, doi:10.1016/j.jiec.2012.01.017.
17. Moradi, G.R.; Yaripour, F.; Vale-Sheyda, P. Catalytic Dehydration of Methanol to Dimethyl Ether over Mordenite Catalysts. *Fuel Process. Technol.* **2010**, *91*, 461–468, doi:10.1016/j.fuproc.2009.12.005.
18. Phung, T.K.; Proietti Hernández, L.; Lagazzo, A.; Busca, G. Dehydration of Ethanol over Zeolites, Silica Alumina and Alumina: Lewis Acidity, Brønsted Acidity and Confinement Effects. *Appl. Catal. Gen.* **2015**, *493*, 77–89, doi:10.1016/j.apcata.2014.12.047.
19. Sepehrian, H.; Khanchi, A.R.; Rofouei, M.K.; Waqif Husain, S. Non-Thermal Synthesis of Mesoporous Zirconium Silicate and Its Characterization. *J. Iran. Chem. Soc.* **2006**, *3*, 253–257, doi:10.1007/BF03247216.
20. De Souza, L.K.C.; Pardauil, J.J.R.; Zamian, J.R.; Da Rocha Filho, G.N.; Da Costa, C.E.F. Influence of the Incorporated Metal on Template Removal from MCM-41 Type Mesoporous Materials. *J. Therm. Anal. Calorim.* **2011**, *106*, 355–361, doi:10.1007/s10973-011-1295-1.
21. Occelli, M.L.; Biz, S.; Auroux, A. Effects of Isomorphous Substitution of Si with Ti and Zr in Mesoporous Silicates with the MCM-41 Structure. *Appl. Catal. Gen.* **1999**, *183*, 231–239, doi:10.1016/S0926-860X(99)00059-9.

22. Chen, C.-L.; Li, T.; Cheng, S.; Lin, H.-P.; Bhongale, C.J.; Mou, C.-Y. Direct Impregnation Method for Preparing Sulfated Zirconia Supported on Mesoporous Silica. *Microporous Mesoporous Mater.* **2001**, *50*, 201–208, doi:10.1016/S1387-1811(01)00453-X.
23. Ghorbani, F.; Habibollah Younesi; Mehraban, Z.; Çelik, M.S.; Ghoreyshi, A.A.; Anbia, M. Preparation and Characterization of Highly Pure Silica from Sedge as Agricultural Waste and Its Utilization in the Synthesis of Mesoporous Silica MCM-41. *J. Taiwan Inst. Chem. Eng.* **2013**, *44*, 821–828, doi:10.1016/j.jtice.2013.01.019.
24. Kim, J.; Yong, K. Characterization of Hafnium Silicate Thin Films Grown by MOCVD Using a New Combination of Precursors. *J. Cryst. Growth* **2004**, *263*, 442–446, doi:10.1016/j.jcrysgro.2003.12.009.
25. Leofanti, G.; Padovan, M.; Tozzola, G.; Venturelli, B. Surface Area and Pore Texture of Catalysts. *Catal. Today* **1998**, *41*, 207–219, doi:10.1016/S0920-5861(98)00050-9.
26. Hong, G.-B.; Ruan, R.-T.; Chang, C.-T. MCM-41 from Spent Glasses for Volatile Organic Compounds Treatment. *Chem. Eng. J.* **2013**, *215–216*, 472–478, doi:10.1016/j.cej.2012.09.128.
27. Mahendran, N.; Johnson Jeyakumar, S.; Jothibas, M.; Ponnar, M.; Muthuvel, A. Synthesis, Characterization of Undoped and Copper-Doped Hafnium Oxide Nanoparticles by Sol–Gel Method. *J. Mater. Sci. Mater. Electron.* **2022**, *33*, 10439–10449, doi:10.1007/s10854-022-08031-0.
28. Guo, Q.; Wang, T. Preparation and Characterization of Sodium Sulfate/Silica Composite as a Shape-Stabilized Phase Change Material by Sol-Gel Method. *Chin. J. Chem. Eng.* **2014**, *22*, 360–364, doi:10.1016/S1004-9541(14)60047-1.
29. Pizzio, L.R.; Vázquez, P.G.; Cáceres, C.V.; Blanco, M.N. Supported Keggin Type Heteropolycompounds for Ecofriendly Reactions. *Appl. Catal. Gen.* **2003**, *256*, 125–139, doi:10.1016/S0926-860X(03)00394-6.
30. Jung, S.M.; Grange, P. TiO_2–SiO_2 Mixed Oxide Modified with H_2SO_4. *Appl. Catal. Gen.* **2002**, *228*, 65–73, doi:10.1016/S0926-860X(01)00960-7.
31. Alharbi, W.; Brown, E.; Kozhevnikova, E.F.; Kozhevnikov, I.V. Dehydration of Ethanol over Heteropoly Acid Catalysts in the Gas Phase. *J. Catal.* **2014**, *319*, 174–181, doi:10.1016/j.jcat.2014.09.003.
32. Zhang, X.; Wang, R.; Yang, X.; Zhang, F. Comparison of Four Catalysts in the Catalytic Dehydration of Ethanol to Ethylene. *Microporous Mesoporous Mater.* **2008**, *116*, 210–215, doi:10.1016/j.micromeso.2008.04.004.
33. Sheng, Q.; Ling, K.; Li, Z.; Zhao, L. Effect of Steam Treatment on Catalytic Performance of HZSM-5 Catalyst for Ethanol Dehydration to Ethylene. *Fuel Process. Technol.* **2013**, *110*, 73–78, doi:10.1016/j.fuproc.2012.11.004.
34. Said, A.E.-A.A.; Abd El-Wahab, M.M.; El-Aal, M.A. The Catalytic Performance of Sulfated Zirconia in the Dehydration of Methanol to Dimethyl Ether. *J. Mol. Catal. Chem.* **2014**, *394*, 40–47, doi:10.1016/j.molcata.2014.06.041.
35. Yaripour, F.; Baghaei, F.; Schmidt, I.; Perregaard, J. Catalytic Dehydration of Methanol to Dimethyl Ether (DME) over Solid-Acid Catalysts. *Catal. Commun.* **2005**, *6*, 147–152, doi:10.1016/j.catcom.2004.11.012.